ARMY RESEARCH LABORATORY

Z-scan Measurement of the Upconversion Coefficient in Er:YAG

by Jeffrey O. White, Robert Dibiano, Alexander B. Fick, and John E. McElhenny

ARL-TR-4994 **September 2009**

NOTICES

Disclaimers

The findings in this report are not to be construed as an official Department of the Army position unless so designated by other authorized documents.

Citation of manufacturer's or trade names does not constitute an official endorsement or approval of the use thereof.

Destroy this report when it is no longer needed. Do not return it to the originator.

Army Research Laboratory
Adelphi, MD 20783-1197

ARL-TR-4994 **September 2009**

Z-scan Measurement of the Upconversion Coefficient in Er:YAG

Jeffrey O. White, Robert Dibiano, Alexander B. Fick, and John E. McElhenny
Sensors and Electron Devices Directorate, ARL

REPORT DOCUMENTATION PAGE	Form Approved OMB No. 0704-0188

1. REPORT DATE *(DD-MM-YYYY)*	2. REPORT TYPE	3. DATES COVERED (From - To)
September 2009	Final	June 2008 to August 2009

4. TITLE AND SUBTITLE

Z-scan Measurement of the Upconversion Coefficient in Er:YAG

5a. CONTRACT NUMBER

5b. GRANT NUMBER

5c. PROGRAM ELEMENT NUMBER

6. AUTHOR(S)

Jeffrey O. White, Robert Dibiano, Alexander B. Fick, and John E. McElhenny

5d. PROJECT NUMBER

5e. TASK NUMBER

5f. WORK UNIT NUMBER

7. PERFORMING ORGANIZATION NAME(S) AND ADDRESS(ES)

U.S. Army Research Laboratory
ATTN: RDRL-SEE-O
2800 Powder Mill Road
Adelphi, MD 20783-1197

8. PERFORMING ORGANIZATION REPORT NUMBER

ARL-TR-4994

9. SPONSORING/MONITORING AGENCY NAME(S) AND ADDRESS(ES)

10. SPONSOR/MONITOR'S ACRONYM(S)

11. SPONSOR/MONITOR'S REPORT NUMBER(S)

12. DISTRIBUTION/AVAILABILITY STATEMENT

Approved for public release; distribution unlimited.

13. SUPPLEMENTARY NOTES

14. ABSTRACT

Solid-state laser research at the U.S. Army Research Laboratory (ARL) is currently emphasizing techniques for power scaling and achieving wavelengths in the eye-safer spectral region. We are studying erbium-doped yttrium aluminum garnet (Er:YAG), because it can be operated with a low quantum defect and has transitions around 1.6 μm. However, it suffers from cooperative pair upconversion, which can raise the lasing threshold, and thus lower the output power. In this report, we demonstrate how to measure the upconversion coefficient C_{up} using the z-scan technique with a continuous wave source. We find C_{up} to be proportional to [Er], for concentrations ranging from 0.5–5%. The value we find at 1% is 3.6×10^{-17} cm^3/s, approximately eight times larger than a value reported previously in the literature.

15. SUBJECT TERMS

ER:YAG, upconversion, z-scan

16. SECURITY CLASSIFICATION OF:			17. LIMITATION OF ABSTRACT	18. NUMBER OF PAGES	19a. NAME OF RESPONSIBLE PERSON
a. REPORT	b. ABSTRACT	c. THIS PAGE			Jeffrey O. White
Unclassified	Unclassified	Unclassified	UU	20	19b. TELEPHONE NUMBER (*Include area code*) (301) 394-0069

Standard Form 298 (Rev. 8/98)
Prescribed by ANSI Std. Z39.18

Contents

List of Figures

Summary

In a solid-state laser, cooperative upconversion can be beneficial or deleterious, i.e., it can populate or de-populate the upper laser level, depending on the ion and transitions involved. In the case of erbium-doped yttrium aluminum garnet (Er:YAG), at excitation densities typically occurring in our lasers, the dominant upconversion process occurs when two ions in the first excited manifold $^4I_{13/2}$ are in close proximity. This competes with stimulated emission from the $^4I_{13/2}$ manifold. The coefficient that characterizes this process has been measured in the past with pulsed sources by examining the non-exponential decay of fluorescence from the various levels involved. We propose a steady-state technique for measuring the upconversion coefficient that uses the same continuous wave (CW) source that is used to pump an Er:YAG laser. We find that C_{up} is proportional to [Er], as expected, but approximately eight times larger than previously reported values.

INTENTIONALLY LEFT BLANK.

1. Introduction/Background

Er:YAG is a promising material for eye-safer lasers because emission from the $^4I_{13/2}$ manifold is in the 1.6-µm spectral region. Er:YAG can also address the need for a low quantum defect, because the crystal field splitting is large enough at 300 K that one can pump and lase between the lowest two manifolds. The energy levels in the lowest four manifolds are shown in figure 1.

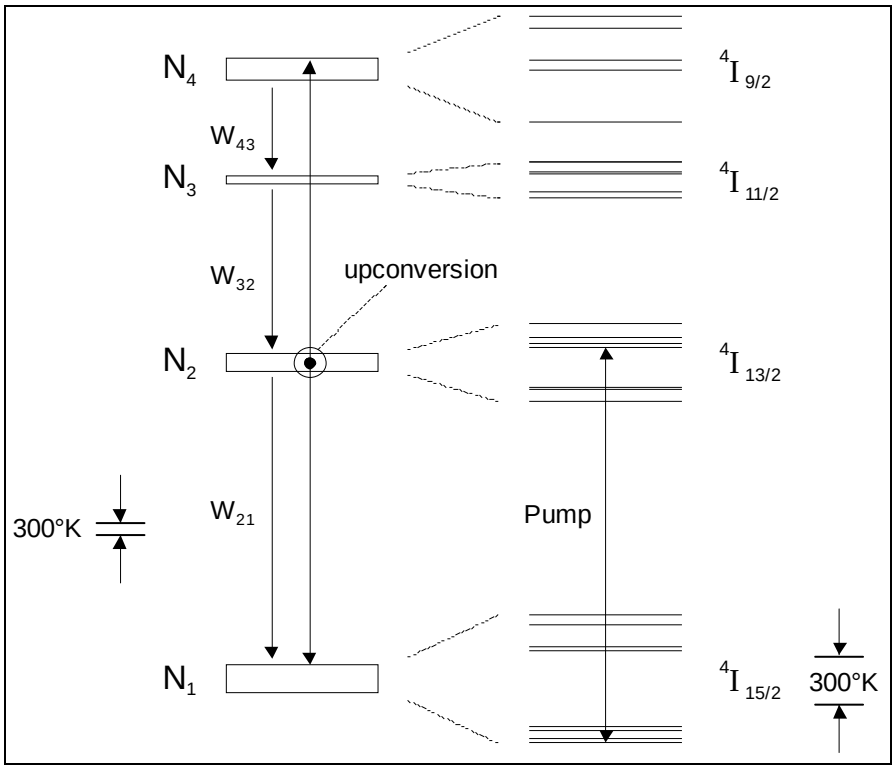

Figure 1 Energy levels in the lowest four manifolds of Er:YAG. The scale on the right is magnified.

When pumped at 1532 nm at room temperature, Er:YAG lases at 1645 nm, representing a quantum defect of about 7%. A small quantum defect is advantageous for high average power lasers, where heat generation is proportional to the input power and quantum defect. However the upper laser level can be depleted by cooperative pair upconversion (CPU), because the $^4I_{9/2}$ manifold in Er:YAG is at 12301–12760 cm^{-1}, about twice the energy of the $^4I_{13/2}$ manifold at 6544–6879 cm^{-1}. In this (lowest order) process, the electron in one ion jumps to the $^4I_{9/2}$ manifold and the electron in the other ion returns to the ground state $^4I_{15/2}$ manifold.

Higher order upconversion also occurs. For example, when Er:YAG is pumped at 1532 nm, green light is emitted at ~500 nm. Although it is possible for multiple photons to excite a single ion in stepwise fashion before it relaxes, the majority of Er ions above the $^4I_{13/2}$ manifold arrive there through a cooperative process (*1*).

2. Experiment/Calculations

The schematic for the experimental setup is shown in figure 2. A 5-MHz linewidth distributed feedback Bragg (DFB) laser diode is temperature tuned to resonance with the 1532-nm Er absorption line (figure 3). It seeds the Er fiber amplifier with 14 mW. The 1–3 W output of the amplifier is collimated, chopped, and focused, then passes through the sample before falling on an indium gallium arsenide (InGaAs) photodiode connected to a lock-in amplifier (LIA). The optical chopper reduces the duty cycle to 10%, to minimize sample heating. The intensity can be varied over a factor of 10 by changing the power of the beam, but it can be varied by 3–4 orders of magnitude by translating the sample axially through the focus. The Er concentration was varied from 0.5–5% by using different samples of 1-mm thickness and 10-mm diameter (*2*). The samples are anti-reflection coated on both sides.

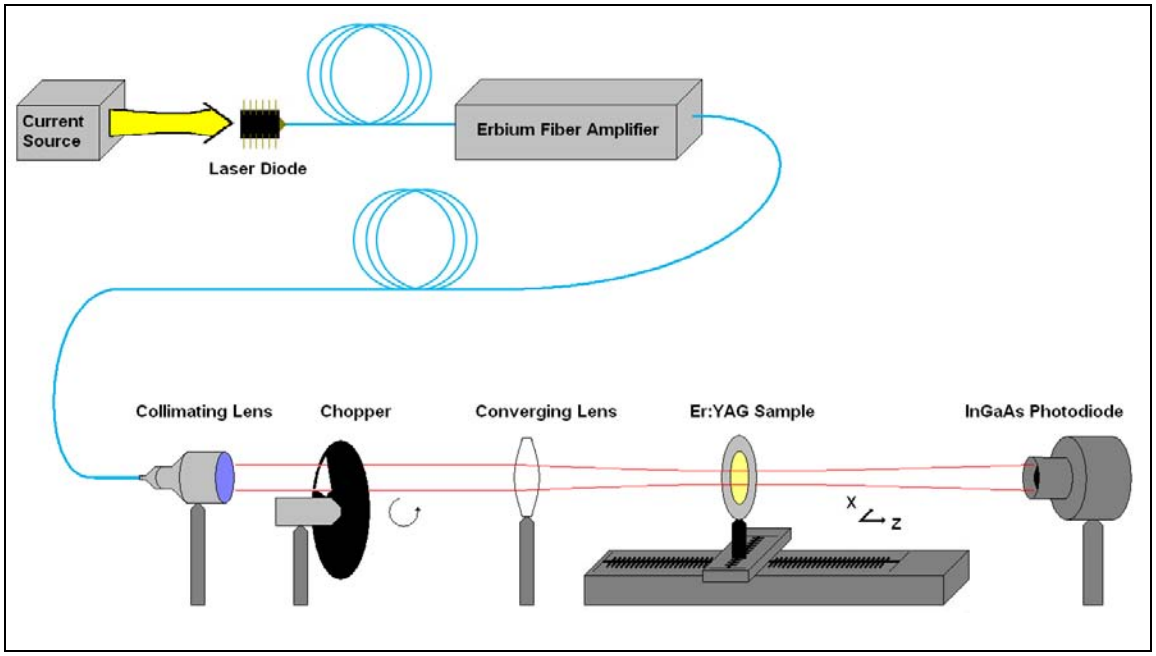

Figure 2. Experimental setup.

With the sample removed, the photodiode measures the incident power. With the sample in place, the motorized stage moves in the z-direction through the focus with steps of 2 mm, under computer control. Focal lengths of 15 and 20 cm were used. The computer also reads from an analog-to-digital converter connected to the analog output of the LIA. Room light and upconversion fluorescence light are blocked by a long-wave-pass filter. A diffuser and a series of neutral density filters in front of the photodiode reduce the current to ~0.2 µA, a level that can be handled by the LIA.

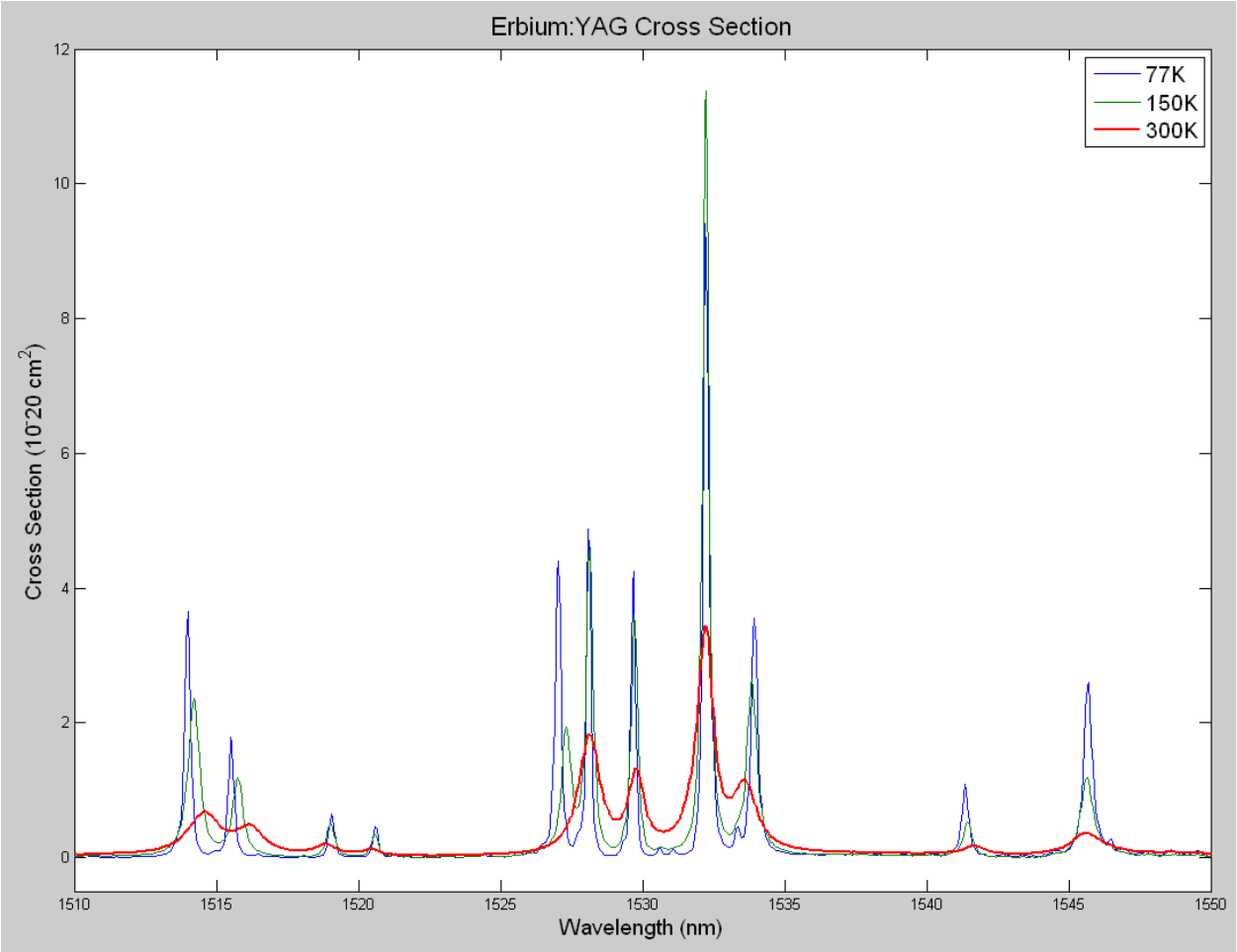

Figure 3. Absorption cross section of Er:YAG for a range of crystal temperatures.

A preliminary run is made to determine the intensity profile of the beam at each z position. These data were obtained by measuring the transmitted power when a razor blade was translated across the beam in the x direction. The transmitted power corresponds to an integral over a half-space of the two-dimensional Gaussian intensity profile. This reduces to the cumulative distribution function, equation 1 (*3*). The beam radius, w, is obtained by fitting the experimental data to equation 2. P is the total incident power.

$$p = F(x|\mu,w) = \frac{1}{w\sqrt{2\pi}}\int_{-\infty}^{x}\exp[\frac{-(t-\mu)^2}{2w^2}]dt \quad (1)$$

$$q = P[1-F(x|\mu,w)] \quad (2)$$

The theoretical equation for a TEM_{00} Gaussian beam radius in homogeneous media (*4*) was then fit to the data (figure 4). The good fit indicates a fundamental Gaussian beam.

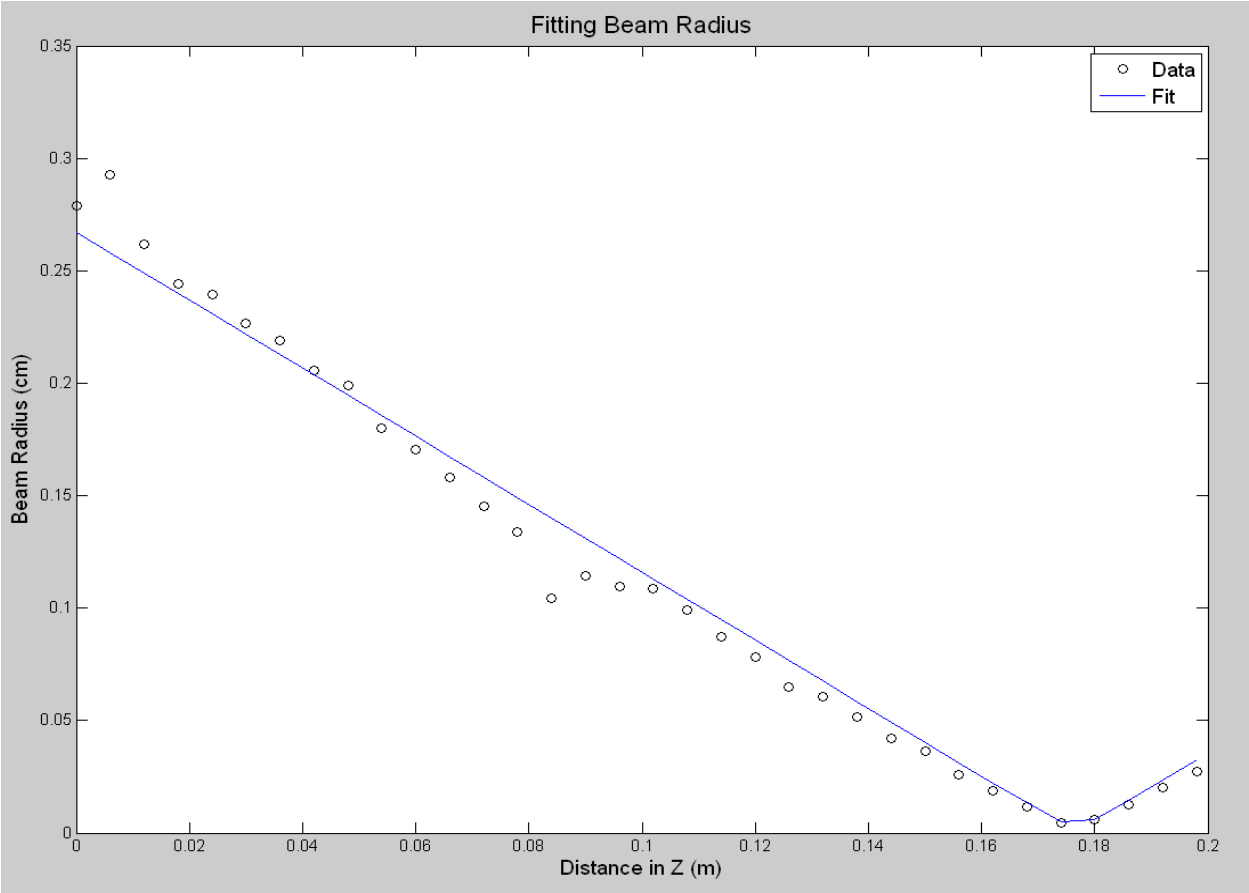

Figure 4. Beam radius data and a least squares theoretical fit for the 20-cm lens.

$$w^2(z) = w_0^2 \cdot \left[1 + \left(\frac{z}{z_0}\right)^2\right] \tag{3}$$

Next, a nominal upconversion value $\tilde{C}_{up}$ was obtained from the literature (*1*). For each sample $\tilde{C}_{up}$ is calculated from equation 4. The relation is simply a proportionality constant relating the upconversion rate to the density of Er ions.

$$\tilde{C}_{up} = 3.6\times10^{-38} f_{Er} N_Y \qquad N_Y = 3N_{Av}\frac{\rho_{YAG}}{3M_Y + 5M_{Al} + 12M_O} \tag{4}$$

The theoretical transmission curve as a function of z was calculated for a few multiples of $\tilde{C}_{up}$. The model that follows assumes a uniform intensity (plane wave); therefore, the Gaussian profile has to be simulated as a superposition of different intensities, each propagated separately through the sample.

The plane wave model includes rate equations for the lowest four manifolds of Er^{3+}, grouping together the population of each manifold.

$$\frac{dN_1}{dt} = +\frac{I_p \sigma_p}{h\nu_p}\left(f_{ep} N_2 - f_{ap} N_1\right) + N_2 W_{21} + N_3 W_{31} + N_4 W_{41} + C_{up} N_2^2 . \quad (5)$$

$$\frac{dN_2}{dt} = -\frac{I_p \sigma_p}{h\nu_p}\left(f_{ep} N_2 - f_{ap} N_1\right) - N_2 W_{21} + N_3 W_{32} + N_4 W_{42} - 2C_{up} N_2^2 \quad (6)$$

$$\frac{dN_3}{dt} = N_4 W_{43} - N_3\left(W_{32} + W_{31}\right) \quad (7)$$

$$\frac{dN_4}{dt} = C_{up} N_2^2 - N_4\left(W_{43} + W_{42} + W_{41}\right) \quad (8)$$

Here, N_1 is the population of the lowest $^4I_{15/2}$ level, I_P is the pump intensity, σ_P is the absolute cross section, f_{ep} (f_{ap}) is the probability that an electron is in a state that can emit (absorb) a pump photon, W_{ij} is the relaxation rate from level i to level j, and C_{up} is the upconversion parameter. Also included in the model is a propagation equation for the pump beam:

$$\frac{dI_p}{dz} = \quad I_p \sigma_p \left(f_{ep} N_2 - f_{ap} N_1\right) = -\alpha_p I_p . \quad (9)$$

Equations 5–9 are solved in steady state using MATLAB®. The effective absorption coefficient α_{eff} is calculated from the transmission data, using equation 10:

$$I_p(L) = I_p(0)\exp\left(-\alpha_{eff} L\right) \quad (10)$$

There are a number of assumptions made in this experiment and its analysis. First, the beam radius is assumed to be constant throughout the 1-mm thickness of the sample. This makes the intensity and transmission calculations much easier, and is supported by all samples having a thickness smaller than the confocal parameter, or Rayleigh range. Another assumption is that scattering losses were negligible. This is well-justified by the excellent optical quality of the sample. As stated previously, the mathematical model only accounts for CPU to the $^4I_{9/2}$ manifold; we neglect the effect of multiple photons exciting a single ion or CPU occurring to higher energy states. The model is also "local" in the sense that the populations at any point in space are determined by the intensity at that point. This assumes that the excitations only migrate distances that are short compared to the beam diameter.

3. Results and Discussion

The z-scan results for transmission as a function of z show a peak where the beam intensity is highest, due to saturation of the absorption (figure 5b). The effect of upconversion is to shift the onset of saturation to higher intensities, because it depletes the $^4I_{13/2}$ manifold. The shift of saturation can be seen more clearly in a plot of α_{eff} versus peak intensity (figure 5c). The experimental data indicate a value of C_{up} that is approximately eight times larger than that reported in the literature. We estimate the accuracy to be a factor of two.

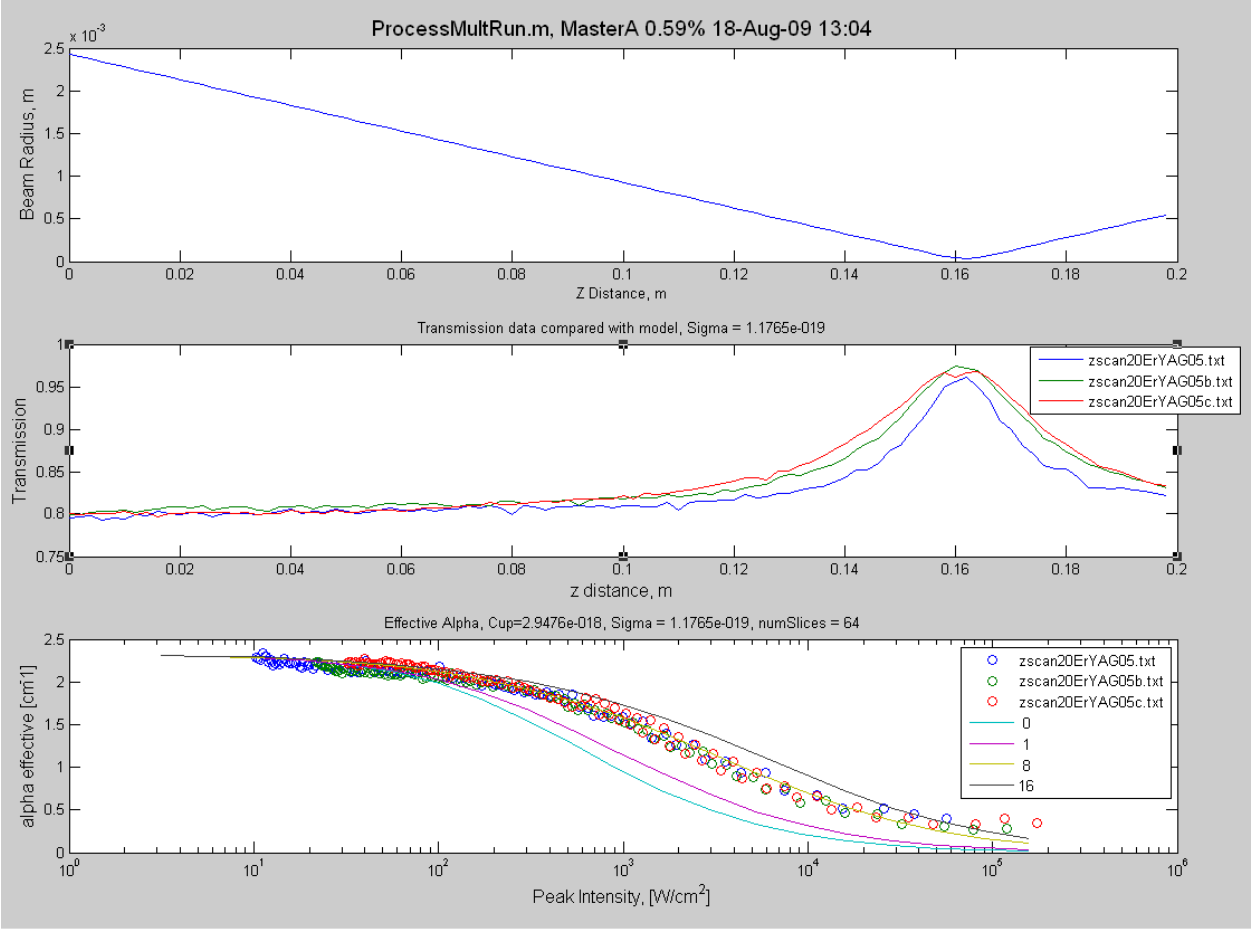

Figure 5. (a) Beam radius as a function of z, (b) transmission as a function of z, and (c) effective absorption coefficient as a function of peak intensity. Three runs at 1, 2, and 3 W are combined on the bottom two graphs.

The values we obtain for C_{up} are 2.3×10^{-17} cm^3/s for the 0.57% sample, and 4.4×10^{-17} cm^3/s for the 1.1% sample. The nominal concentrations are 0.5% and 1%. We adjusted the concentrations slightly to match the linear absorption, while keeping the cross section at its nominal value of 1.18×10^{-19} cm^2. For low concentrations, C_{up} is proportional to concentration, as expected (1) (figure 6).

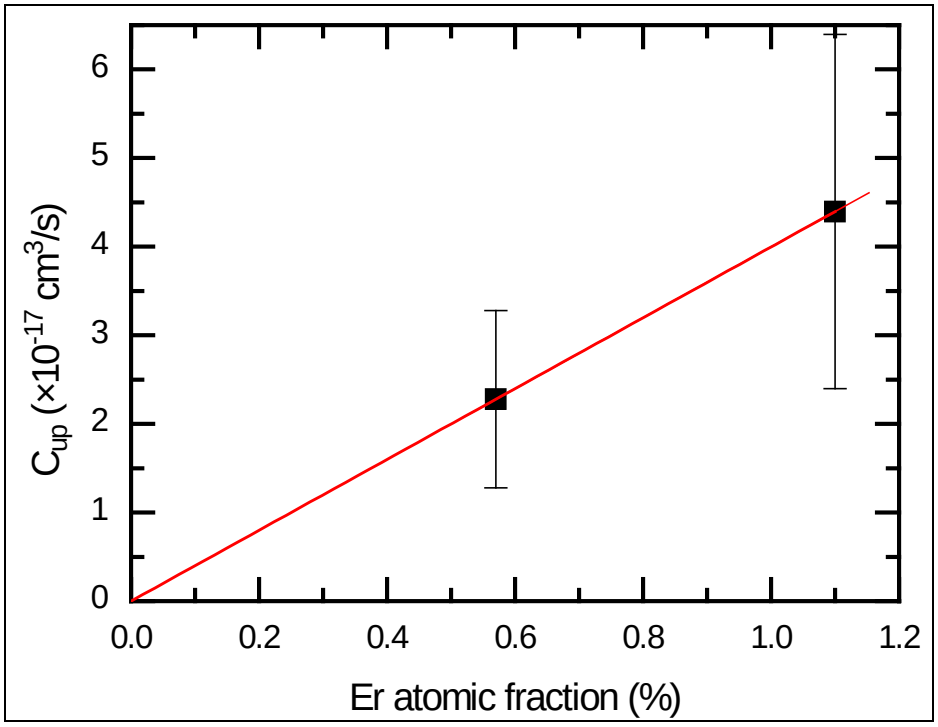

Figure 6. Upconversion coefficient as a function of Er atomic fraction at room temperature.

Using the simulation and $C_{up} = 8\tilde{C}_{up}$, it is possible to plot the losses due to upconversion as a function of both intensity and erbium concentration. Increasing either intensity or [Er] resulted in more loss, as seen in figure 7. The upconversion seems to scale linearly with [Er], although its relationship with peak intensity is more complicated.

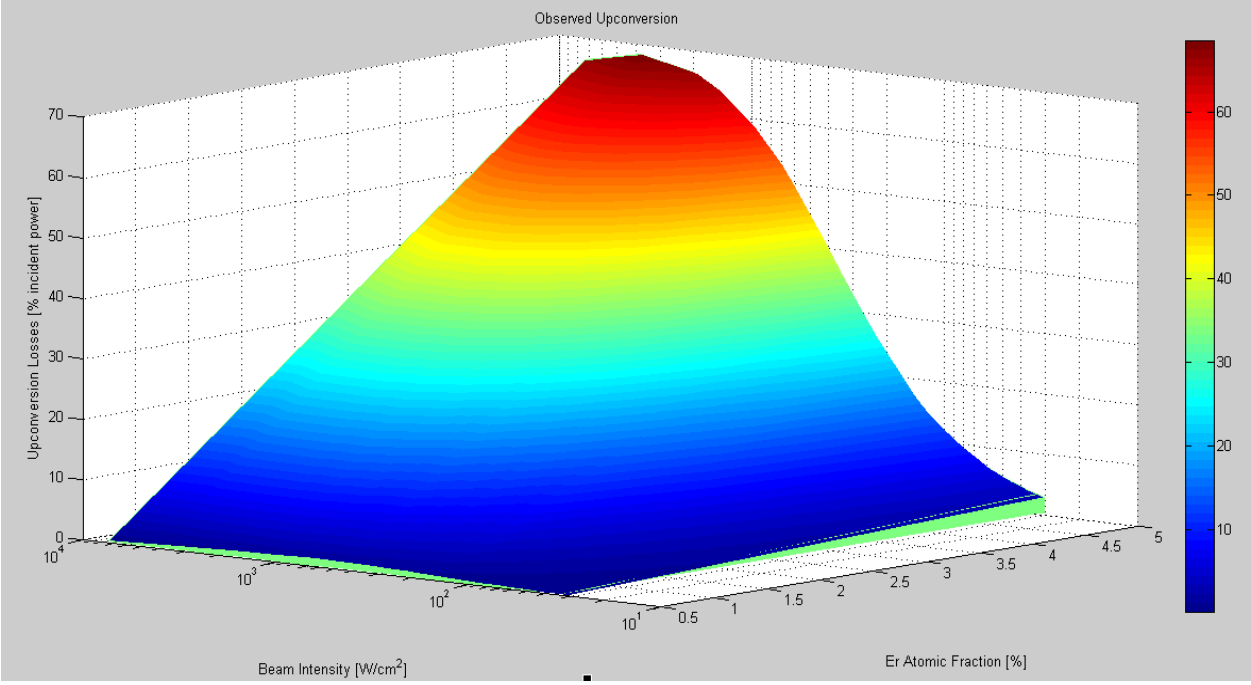

Figure 7. Losses due to upconversion as a function of both erbium doping and beam peak intensity. Increasing either [Er] or peak intensity will cause more upconversion until a maximum upconversion rate has been reached.

4. Summary and Conclusions

In an Er:YAG laser operating at 1645 nm, no upconversion would ideally take place, and the pump photons would have a 1:1 ratio with emitted photons. The only non-negligible heat generation would be from phonons that make up the quantum defect. The presence of upconversion causes more heat generation and lowers the power of the emitted laser beam, putting an upper bound on the allowable pump beam intensity and [Er], both of which introduce limits in creating a high energy laser. The results of the experiment show that the assumptions made were justified, that the experimental setup is effective at producing reliable information about the behavior of upconversion in Er:YAG, and that upconversion increases with [Er] and beam intensity.

5. References

1. Iskandarov, M. O.; Nikitichev, A. A.; Stepanov, A. I. *J. Opt. Technol.* **2001**, *68*, 885.
2. Scientific Materials, Inc., Bozeman, MT.
3. NIST/SEMATECH e-Handbook of Statistical Methods, 1.3.6.7.1, 2006.
4. Yariv, A. *Quantum Electronics* **1975**, *111*.
5. White, J. O.; Dubinskii, M.; Merkle, L. D.; Kudryashov, I.; Garbuzov, D. *J. Opt. Soc. Am. B.* **2007**, *24*, 2454.

Symbols, Abbreviations, and Acronyms

CPU	cooperative pair upconversion
CW	continuous wave
DFB	distributed feedback Bragg (laser)
Er	erbium
InGaAs	indium gallium arsenide
LIA	lock-in amplifier
TEM_{00}	transverse electromagnetic, fundamental mode
YAG	yttrium aluminum garnet

No. of Copies	Organization
1 ELECT	ADMNSTR DEFNS TECHL INFO CTR ATTN DTIC OCP 8725 JOHN J KINGMAN RD STE 0944 FT BELVOIR VA 22060-6218
1	DARPA ATTN IXO S WELBY 3701 N FAIRFAX DR ARLINGTON VA 22203-1714
1 CD	OFC OF THE SECY OF DEFNS ATTN ODDRE (R&AT) (1 CD) THE PENTAGON WASHINGTON DC 20301-3080
1	US ARMY RSRCH DEV AND ENGRG CMND ARMAMENT RSRCH DEV AND ENGRG CTR ARMAMENT ENGRG AND TECHNLGY CTR ATTN AMSRD AAR AEF T J MATTS BLDG 305 ABERDEEN PROVING GROUND MD 21005-5001
1	PM TIMS, PROFILER (MMS-P) AN/TMQ-52 ATTN B GRIFFIES BUILDING 563 FT MONMOUTH NJ 07703
1	US ARMY INFO SYS ENGRG CMND ATTN AMSEL IE TD A RIVERA FT HUACHUCA AZ 85613-5300
1	COMMANDER US ARMY RDECOM ATTN AMSRD AMR W C MCCORKLE 5400 FOWLER RD REDSTONE ARSENAL AL 35898-5000

No. of Copies	Organization
1	US GOVERNMENT PRINT OFF DEPOSITORY RECEIVING SECTION ATTN MAIL STOP IDAD J TATE 732 NORTH CAPITOL ST NW WASHINGTON DC 20402
1	US ARMY RSRCH LAB ATTN RDRL CIM G T LANDFRIED BLDG 4600 ABERDEEN PROVING GROUND MD 21005-5066
15	US ARMY RSRCH LAB ATTN IMNE ALC HRR MAIL & RECORDS MGMT ATTN RDRL CIM L TECHL LIB ATTN RDRL CIM P TECHL PUB ATTN RDRL SEE O J E MCELHENNY ATTN RDRL SEE O J WHITE (6 COPIES) ATTN RDRL SEE O J ZHANG ATTN RDRL SEE O L MERKLE ATTN RDRL SEE O M DUBINSKIY ATTN RDRL SEE O N TER-GABRIELYAN ATTN RDRL SEE O T SANAMYAN ADELPHI MD 20783-1197
TOTAL:	24 (1 ELECT, 1 CD 22 HCS)

INTENTIONALLY LEFT BLANK.